

On the inception of streamers from sprite halo events produced by lightning discharges with positive and negative polarity

Jianqi Qin,¹ Sebastien Celestin,¹ and Victor P. Pasko¹

Received 9 December 2010; revised 3 February 2011; accepted 1 March 2011; published 3 June 2011.

[1] In the sprite halo events produced by cloud-to-ground lightning discharges, the spatial offsets, long delays, and polarity asymmetry related to the inception of sprite streamers are yet to be explained consistently with observations. In the present work, we use a two-dimensional model and a high-resolution one-dimensional plasma fluid model accounting for electron impact ionization, dissociative attachment, and photoionization processes to simulate halo events. In order to monitor the inception of sprite streamers, that cannot be modeled with present computer resources in the framework of fluid models, we use an improved avalanche-to-streamer transition criterion and investigate the response of the lower ionosphere to the charge moment changes induced by lightning discharges as a system of avalanches. On the basis of simulation results, we suggest a new mechanism for the inception of sprite streamers, explaining specifically how they can be triggered spatially outside of and temporally separated from the main sprite halo. The inception of sprite streamers is demonstrated to depend strongly on the charge moment change and the ambient electron density profile, which together determine the size of the streamer initiation region. We show that sprite streamers are mostly triggered by positive cloud-to-ground lightning discharges mainly because of mechanisms related to direction of propagation of electron avalanches. Moreover, the triggering of long-delayed sprites is demonstrated to be a unique property of halos produced by positive cloud-to-ground lightning discharges due to the formation of a long-lasting high-field region. Lightning continuing current can enlarge this high-field region and pull it down to lower altitudes where electron density is lower, extending the streamer initiation region.

Citation: Qin, J., S. Celestin, and V. P. Pasko (2011), On the inception of streamers from sprite halo events produced by lightning discharges with positive and negative polarity, *J. Geophys. Res.*, 116, A06305, doi:10.1029/2010JA016366.

1. Introduction

[2] Sprites [Sentman *et al.*, 1995] are transient luminous events (TLEs) that have attracted extensive interest since their first video documentation by Franz *et al.* [1990]. These fine structured optical phenomena are composed of filamentary streamers occurring at mesospheric altitudes usually following intense positive cloud-to-ground (+CGs) lightning discharges [Stanley *et al.*, 1999; Gerken *et al.*, 2000]. Photometric and high-speed video studies show that sprite streamers are often, but not always, preceded by brief descending glows with lateral extent 40–70 km called sprite halos [Barrington-Leigh *et al.*, 2001; Wescott *et al.*, 2001; Miyasato *et al.*, 2002; Cummer *et al.*, 2006; Stenbaek-Nielsen and McHarg, 2008].

[3] Horizontal spatial offsets between sprite streamers and the related halo associated with the underlying lightning

discharges have been studied by Wescott *et al.* [2001], McHarg *et al.* [2002], and Moudry *et al.* [2003]. Wescott *et al.* [2001] documented that horizontal position of sprites with vertical columnar structure can be laterally offset by as much as 50 km from the underlying +CGs, whereas sprite halos are observed to be centered directly over the +CGs. In the work of Wescott *et al.* [2001], thirteen discrete sprites following three halos were not centered directly above the +CGs but located at a mean distance of 25.2 km with a standard deviation of 18.8 km.

[4] Vertical offsets between the inception of sprite streamers and related halos have been observed using a high-speed intensified CCD imager with 1 ms time resolution by McHarg *et al.* [2002] and Moudry *et al.* [2003]. Observations clearly show that sprite streamers can be triggered outside of the main halo and subsequently propagate with filamentary part downward and diffuse part upward.

[5] The characteristics of sprite halos and their temporal relationships to sprite streamers have been studied by Miyasato *et al.* [2002] using a high-speed vertical array photometer, with time resolution 50 μ s, and an image-intensified CCD camera, with a time resolution 16.7 ms. The results indicate that spatiotemporal structure of halos

¹Communications and Space Sciences Laboratory, Department of Electrical Engineering, Penn State University, University Park, Pennsylvania, USA.

produced by both positive and negative CGs are very similar. Since halo luminosity decays significantly before streamer luminosity emerges, the peaks of halo luminosity and streamer luminosity are separated by approximately 2 ms [Miyasato *et al.*, 2002]. This temporal delay between sprite and the related halo appears to be consistent with similar observations reported by Stanley *et al.* [2000], Barrington-Leigh *et al.* [2001], and Wescott *et al.* [2001]. The horizontal, vertical and temporal separation of sprite streamers with respect to sprite halos documented in the literature discussed above provides an observational evidence indicating that the emergence of sprite streamers does not represent a continuous process of halo development.

[6] The temporal delay between the occurrence of sprites and the onset of the causative lightning return stroke is another important characteristic for the understanding of sprite phenomenology. It is well known that the so-called long-delayed sprites can be initiated more than 100 ms after a return stroke, followed by additional removal of thundercloud charge by continuing lightning current [Bell *et al.*, 1998; Cummer and Fullekrug, 2001]. Coordinated analysis of sprites using high-speed images and simultaneous detection of related VLF and ELF electromagnetic fields by Li *et al.* [2008] further demonstrated that, in some cases, intense continuing current following the initial removal of charge from the thundercloud initiates long-delayed sprites. In fact, these authors discovered that in some sprite events the continuing current provides up to 90% of the total charge moment change. The charge moment change Qh_Q is defined as the amount of charge Q transferred to ground by the lightning discharge times the altitude h_Q from which the charge was removed. The quasi-static electric field produced above the thunderstorm is proportional to the total charge moment change [Pasko *et al.*, 1997].

[7] The polarity independence in the ability of +CGs and -CGs to trigger sprite streamers has been reported in some early and more recent numerical models of sprites and sprite halos [Pasko *et al.*, 1997, 1998; Asano *et al.*, 2008, 2009]. However, in contrast to the abundant observations of sprites with extensive vertical structures triggered by +CGs (positive sprites), sprites triggered by -CGs (negative sprites) are extremely rare. Negative sprites were unambiguously identified by Barrington-Leigh *et al.* [1999] and Taylor *et al.* [2008] for only three events. All of these events were short-delayed sprites following the return strokes within 5 ms and triggered by -CGs with very high charge moment changes Qh_Q (-1550, -1380 and -503 C km). One important reason for the rarity of negative sprites is that -CGs usually involve much lower Qh_Q than +CGs [e.g., Pasko *et al.*, 2000]. Indeed, although -CGs are much more numerous than +CGs [e.g., Newsome and Inan, 2010], the ratio of -CGs to +CGs leading to charge moment changes higher than 600 C km is roughly 1/30 [e.g., Cummer and Lyons, 2005]. Nevertheless, halos generated by +CGs and -CGs occur with almost the same frequency for a given lightning current [Newsome and Inan, 2010], whereas the occurrence ratio of positive to negative sprites with well developed streamer structure is more than 1000 to 1 [Williams *et al.*, 2007]. The problem of strong asymmetry between +CGs and -CGs in the triggering of sprite streamers has not been resolved yet, and investigation of related processes represents one of the goals of the present work.

[8] Although the continuing current is usually required to trigger sprites if lightning return stroke removes only a small amount of charge from thundercloud, Hu *et al.* [2002] reported that charge moment changes as low as 120 C km related to +CGs can trigger sprites with delays shorter than 6 ms. Up until now, numerical models have been unsuccessful in describing the inception of sprites associated with such low charge moment changes.

[9] Based on observations, which show that the charge moment change threshold for triggering sprite streamers was 600 C km on two nights, while it was 350 C km on another, Cummer and Lyons [2005] have suggested that the variations in conductivity profile in the mesosphere may account for the different threshold. The importance of conductivity profile, and especially the inhomogeneities in the mesospheric conductivity for triggering of sprite streamers, have been indicated by Pasko *et al.* [1996, 1997, 2000]. Stanley *et al.* [2000] noted that electric field required for triggering of daytime sprites is greater than that during nighttime, while the initiation altitude is lower due to greatly enhanced ionospheric conductivity. Moreover, Pasko and Stenbaek-Nielsen [2002] pointed out that the transition altitude between the diffuse and streamer regions of sprites is a sensitive function of the ambient electron density profile. Stenbaek-Nielsen *et al.* [2010b] indicated that the mesospheric conductivity may play an important role in determining the types of sprites observed. All these studies converge toward the fact that conductivity variations in the mesosphere are critical for the initiation of sprite streamers.

[10] Inception of sprite streamers was interpreted as emerging on the axis of symmetry of a halo in low-resolution simulations [Pasko *et al.*, 1996], and recently in high-resolution simulations with a plasma fluid model on a non-uniform, dynamically adapted computational grid [Luque and Ebert, 2009]. In these works, employing the quasi-static electric field from lightning return stroke in the fluid model appears to be an effective way to simulate the sprite halo dynamics. However, this model cannot fully explain the initiation of sprite streamers in the sense that the above reviewed spatial offsets and temporal delays between sprite halos and sprite streamers, long-delayed sprites, polarity asymmetry between +CGs and -CGs, and sprite streamers triggered by +CGs with very low charge moment changes Qh_Q are not reproduced by Pasko *et al.* [1996] or Luque and Ebert [2009], in which optical emissions of the halos and their following on-axis single-headed sprite streamers represent a continuing process.

[11] The purpose of this paper is to bring a new insight into the understanding of the problems related to the inception, the polarity asymmetry, the temporal delays, and the spatial offsets of sprite streamers based on a new approach to modeling of the halo-sprite system.

2. Qualitative Picture of Initiation of Sprite Streamers for Cloud-to-Ground Lightning Discharges With Different Polarities

[12] In this section we provide an outline of the general scenario of formation of sprite streamers created by lightning discharges with different polarities. The described effects are then quantified with specific model results in subsequent sections of this paper. For convenience of reference,

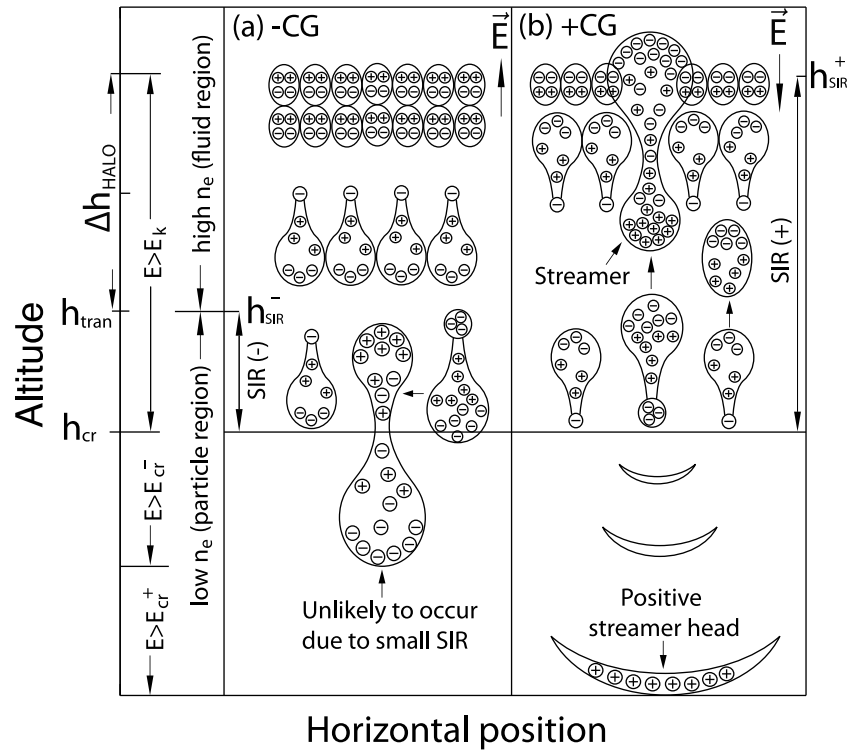


Figure 1. Illustration of sprite halo of both polarities as a system of electron avalanches in the halo high-field region. “SIR” is the streamer initiation region.

important parameters used in the further discussion are summarized in the notation section.

2.1. Electrodynamics Coupling Between Thunderstorm and Ionosphere

[13] The charge moment change Qh_Q produced by a cloud-to-ground lightning discharge with a typical duration τ_l leads to establishment of transient quasi-static electric field E at mesospheric/lower ionospheric altitudes. The electric field E can exceed the threshold field E_k , which is defined by the equality of the ionization and dissociative attachment frequencies [e.g., Raizer, 1991, p. 135], required for avalanche multiplication of electrons. The related altitude range of the $E > E_k$ region is schematically depicted in Figure 1. The lower boundary of this region is due to the increase of E_k proportionally to density of air N at lower altitudes, and is mostly controlled by the charge moment change magnitude Qh_Q and slightly modified by the space charge at the upper boundary (i.e., the halo front) that together define the ratio E/E_k . During the return stroke in the process of charge removal from the thundercloud, the lower boundary is descending due to increasing electric field E . The descending upper boundary of the $E > E_k$ region is defined by the fast relaxation of the applied electric field E that proceeds on time scales shorter than the time scale of application of the field (i.e., τ_l). The vertical profile of ambient atmospheric conductivity at these altitudes exhibits fast increase by several orders of magnitude due to the appearance of a large number of free electrons forming the D region of the ionosphere (schematically shown in Figure 1 as high electron density n_e region). The dynamic relaxation of the electric field generally reflects the electrodynamic

response of the conducting atmosphere at different altitudes and leads to downward shift of the upper boundary of the $E > E_k$ region on a submillisecond time scales. The related processes, including electron impact ionization and attachment effects, and optical emissions have been modeled using quasi-static as well as fully electromagnetic models [e.g., Pasko *et al.*, 1997; Barrington-Leigh *et al.*, 2001]. This upper part of sprite phenomenon is usually referred to as a diffuse or halo region of sprites, and the quantitative analysis conducted by Pasko *et al.* [1998] indicated that very fast relaxation of the electric field in comparison with time scale needed for formation of streamers prevents streamers from forming in this region. This phenomenological fact can be understood in terms of overlapping of the numerous avalanches initiated by closely spaced electrons and is schematically illustrated in Figure 1 by a large number of seed electrons near the upper boundary of the $E > E_k$ region. Electron avalanches at these high altitudes cannot develop independently. Instead, they together form a large-scale ionization wave. The situation is different at lower altitudes if the charge moment change Qh_Q is high enough so that the $E > E_k$ region reaches low-conductivity region where the avalanches can develop without overlapping. Indeed, it has been demonstrated that due to the reduction in the number density of ambient electrons, that can also be affected by the electron dissociative attachment processes, the time scale of streamer formation in this region is shorter than the time scales of relaxation of the electric field and individual electron avalanches can develop into streamers [Pasko *et al.*, 1998]. Figure 1 illustrates this by a smaller number of electron seeds near the lower boundary of the $E > E_k$ region. In terms of overlapping, electron

avalanches initiated at these low-conductivity altitudes are able to develop independently, and individually develop the local enhancement of their space-charge field, which eventually leads to filamentary streamers.

2.2. Lightning Polarity Asymmetry in Triggering Sprite Streamers

[14] In order to understand the origin of polarity asymmetry in triggering of sprite streamers by +CGs and -CGs with the same magnitude of charge moment change Qh_Q , it is insightful to consider an imaginary situation where no ionosphere is present (i.e., there are no ambient electrons). In this situation, the appearance of only one seed electron above the lower boundary of the $E > E_k$ region produced by either a +CG or a -CG can easily lead to the formation of a sprite streamer. In other words, the high ambient electron density plays a key role in disabling the streamer formation, without which an avalanche initiated from a single seed electron in the upper atmosphere can develop into a sprite streamer.

[15] It has been well established in the studies of atmospheric pressure glow discharge (APGD) that sufficiently high preionization, corresponding to 10^5 cm^{-3} at ground level atmospheric pressure in the CO_2 laser system and 10^6 – 10^7 cm^{-3} for APGD controlled by dielectric barrier, is critical in order to sustain the discharge as a volume-stabilized diffuse glow rather than filamentary streamers [Palmer, 1974; Massines *et al.*, 1998; Gherardi and Massines, 2001]. In dielectric barrier discharges in nitrogen at atmospheric pressure, decrease of seed electron density can destabilize the glow discharge when the breakdown occurs and lead to a transition to streamer discharge [Gherardi and Massines, 2001]. Sprite halo is similar to the volume-stabilized glow discharge initiated between electrodes at atmospheric pressure, for example, in the CO_2 laser system. In fact, with abundant electron-ion pairs, the lower ionosphere naturally satisfies the requirement for initiating a volume-stabilized glow discharge, for which as stated by Palmer [1974], the preionization is required to be large enough to cause appreciable spatial overlap of the primary avalanches and consequent smoothing of space-charge field gradients at the stage when streamer formation would otherwise occur. Following this statement, we see that sprite streamers occur only if the electron density is low enough so that avalanches do not overlap with each other. It is useful to introduce a parameter h_{tran} that defines the altitude below which the volume-stabilized feature of the ionization wave would disappear when breakdown occurs due to low ambient electron density. In other words h_{tran} is the altitude for which the radius of the avalanches at the moment of avalanche-to-streamer transition is equal to the distance between seed electrons. The quantity h_{tran} therefore represents the altitude below which the initiation of avalanches may eventually lead to the inception of sprite streamers if high enough electric field is applied. Once the avalanche-to-streamer transition occurs, a double-headed streamer is created with its positive head propagating downward and negative head upward from the initial altitude in the case of a positive halo. For short-delayed sprites, h_{tran} is mainly determined by the ambient electron density profile, and slightly depends on the attachment processes. For long-delayed sprites, the situation is more complicated as the attachment processes can greatly

reduce the electron density in a region just ahead/below the halo.

[16] In Figure 1, we assume that a quasi-static electric field produced by either a +CG or a -CG with the same Qh_Q is applied to the atmospheric system instantaneously, and then analyze the response of the upper atmosphere as an avalanche system. Analysis shows that polarity asymmetry in initiation of sprite streamers by lightning discharges with different polarities stems from a spatial effect that is related to the increase of both the ratio E/E_k and ambient electron density. As shown in Figure 1, for both polarities, the electron avalanches initiated in the higher portion of the altitude range Δh_{HALO} overlap in a very short time and then their individual local space-charge field gradients are canceled. Avalanches initiated at the lower portion of the altitude range Δh_{HALO} can develop over a short distance without overlapping. Nevertheless, before creating a significant space-charge field, they also merge with each other and lead to the formation of a smooth diffuse front. Streamer formation only occurs below the altitude h_{tran} where electron density is low enough for the avalanches to develop without overlapping. For the negative case, avalanches initiated below altitude h_{tran} in Figure 1 do not overlap and could potentially transform into streamers. However, as shown in Figure 1a, in comparison with the +CG case, these avalanches have a very limited $E > E_k$ streamer initiation region (SIR) to go across. The production of a significant space-charge field before these avalanches cross the altitude h_{cr} , where E becomes less than E_k , is therefore unlikely. If these avalanches cannot create a high enough space-charge field when they reach the $E < E_k$ region, so that the total field (space-charge field plus the ambient, or Laplacian, field) is higher than E_k , avalanches will stop growing since the attachment process dominates when $E < E_k$. In contrast, for the positive case shown in Figure 1b, although the initial conditions are similar to the negative case, avalanches propagate over a much larger SIR region where the electric field is significant and get amplified enough to reach the transition to streamers. The altitude h_{SIR}^+ is the highest possible limit of the SIR for positive halo, which is defined by the requirement that electron density inside of the upward developing avalanche must be higher than the ambient electron density. In this system, it is important to define a region of space where the electric field is higher than the breakdown field, and where the electron density is low enough to prevent the cancellation of individual space-charge field gradients before the avalanche-to-streamer transition. As already noted above, we name this region the streamer initiation region (SIR). We note that the reduced applied electric field (i.e., E/E_k) increases exponentially with altitude, and the SIR above h_{tran} in the positive case plays an essential role in triggering sprite streamers. Two conditions determine if these avalanches can become streamers. First, the avalanche-to-streamer transition needs to be fulfilled before avalanches reach the end of the $E > E_k$ region. Second, once avalanches approach the high electron density region (i.e., above h_{tran} in Figure 1), the electron density inside the avalanche must be higher than the ambient electron density [Vitello *et al.*, 1994].

[17] Concerning the time sequence, electron avalanches at low altitudes, where streamer formation is allowed, can be initiated as soon as the removal of thundercloud charge

establishes a $E > E_k$ region at these altitudes, meanwhile the upper boundary is descending as a large-scale ionization wavefront. Therefore, the initiation of sprite streamer at low altitudes and the development of upper diffuse glow (i.e., sprite halo) can develop as independent events and do not necessarily need to occur one after another. Nevertheless, the establishment of $E > E_k$ at low altitudes requires time scale of the lightning duration (typically 1 ms), after which avalanche-to-streamer transition at low altitude requires time on the order of several ms that depends on the applied electric field and local air density N (if breakdown occurs at lower altitude, streamers are triggered faster due to high air density N leading to higher ionization frequency). The total dielectric relaxation time (i.e., duration of the halo) of the electric field at high altitudes is slightly longer than the lightning duration. Therefore, sprite streamers usually appear after the fast descending diffuse wave observed as sprite halo. The time separation between these two distinct phenomena depends on the relative position of the upper boundary of low electron density region (i.e., h_{tran} in Figure 1) and the lower boundary of the $E > E_k$ region (i.e., h_{cr} in Figure 1). In the case of $h_{\text{tran}} > h_{\text{cr}}$ (i.e., large charge moment change and low ambient electron density), the time required for streamer initiation at low altitude can be similar to the duration of the sprite halo, leading to triggering of short-delayed (several milliseconds) sprites. In particular, if $h_{\text{tran}} \gg h_{\text{cr}}$, sprite streamers and sprite halo appear simultaneously. In an alternative case of $h_{\text{tran}} < h_{\text{cr}}$ continuing current may lower h_{cr} below h_{tran} after a significant delay, in which situation long-delayed (tens of milliseconds) sprites can be produced.

2.3. Lightning Polarity-Dependent Observational Features of Sprite Streamers

[18] Considering again sprite-halos as a system of avalanches, we can see that the observational features of sprite streamers produced by +CGs and -CGs are different due to different effective $E > E_k$ regions. In the case of a -CG, even if an avalanche initiated at lower altitude of the $E > E_k$ region succeeds to develop into a streamer in such a limited region, the downward head of the streamer would encounter the $E < E_k$ region. Although this head still can further develop in the $E > E_{\text{cr}}$ region (see Figure 1), its luminosity is lower than that of the upward head which again develops in the $E > E_k$ region. As will be discussed in more detail below, the E_{cr}^- in Figure 1 refers to the minimum field required for propagation of negative streamers, and E_{cr}^+ to a similar field for positive streamers [Pasko *et al.*, 2000, and references therein]. This analysis indicates that the upward positive head of a negative sprite streamer should be brighter than the downward negative head, which agrees with the observation of the sprite streamers triggered by a -CG reported by Taylor *et al.* [2008]. In the case of a +CG, the situation is more complicated since avalanche-to-streamer transition occurs far above h_{cr} , which means that both downward positive streamers and upward negative streamers have a region where $E > E_k$ to further develop. Nevertheless, since it is unlikely that a sprite streamer is triggered far above h_{cr} by a -CG because of the limitation due to the overlapping of avalanches discussed above, the downward positive streamers triggered by a +CG benefit from a longer effective

length of the high $E > E_k$ region after the inception than the downward negative streamers triggered by a -CG. Due to the recently identified extremely fast, exponential growth of sprite streamers propagating in fields $E > E_{\text{cr}}$ [Liu *et al.*, 2009], we see that the increase in the effective $E > E_k > E_{\text{cr}}^+$ region also has a critically important impact on the luminosity of sprite streamers.

[19] It is known that streamers, once initiated, can propagate in fields much lower than E_k [Pasko *et al.*, 2000, and references therein]. The ground level value of E_k is approximately 30 kV/cm. The minimum field for propagation of negative streamers E_{cr}^- is approximately 12.5 kV/cm and for positive streamers the related field E_{cr}^+ is approximately 4.4 kV/cm. These reference fields are assumed to scale with altitude proportionally to air density N . The streamer initiated at the bottom of sprite halo driven by -CG (Figure 1a) would have a negative head propagating downward and a positive head propagating upward, while streamer initiated at the bottom of a sprite halo driven by +CG would have positive head propagating downward and negative head propagating upward (Figure 1b). Although both upward going positive head in the -CG case and the upward going negative head in +CG case may form and be observable, the conditions for their propagation may not be as favorable as for downward propagating heads because of the increased ambient electron density and the related fast relaxation of the electric field at high altitudes. It is noted that since E_{cr}^+ is a factor of 3 lower than E_{cr}^- the positive streamers propagating downward in +CG case have approximately 10 km more room in altitude to grow in comparison with downward going negative streamers in the -CG case, as schematically shown in Figure 1 (see also Pasko *et al.* [2000, Figure 1a] showing a representative case of altitude scaling of the critical fields with respect to lightning produced field). Due to the recently experimentally documented exponential growth of streamers in sprites in which their brightness increases by more than 4 orders of magnitude in 1 ms [Stenbaek-Nielsen *et al.*, 2007], it is highly likely that the initiated sprite streamers should go through a stage of acceleration and expansion before their luminosity can be detectable in observations [Liu *et al.*, 2009]. As this stage of streamer growth can be completed in a relatively compact region of space ~ 1 km (see discussion by Liu *et al.* [2009]) it is clear that the downward propagating streamers in the +CG case have advantage to grow and to be observable in comparison with the downward negative streamers in -CG case (as schematically depicted in Figure 1). We note that upward propagating negative streamers have been observed in sprites with some delay with respect of formation of downward positive streamers [Stenbaek-Nielsen *et al.*, 2007; McHarg *et al.*, 2007]. The delay may be related to more favorable conditions for growth of positive streamers as discussed above. Pasko [2010] also noted recently that relatively slow application of the electric field at sprite altitudes (~ 1 ms) [Marshall and Inan, 2006; Hu *et al.*, 2007] may also contribute to predominant initial propagation of positive streamers having the lower propagation threshold. Luque and Ebert [2010] and Li and Cummer [2011] have recently suggested that emergence of secondary negative streamers may be related to the negative charging of the upper section of the downward positive streamer.

2.4. Additional Factors Contributing to Asymmetry of Sprite Streamers Created by Lightning Discharges With Different Polarities

[20] As will be demonstrated in subsequent sections of this paper, the additional quantitative factors contributing to the asymmetry in formation of sprite streamers created by lightning discharges with different polarities include the lower electron density below the sprite halo, higher E/E_k ratio and wider altitude extent of the $E > E_k$ region in the +CG case in comparison with -CG case. The presence of significant inhomogeneities in electron distribution (i.e., localized pockets containing large number of seed electrons) is another important factor defining formation of streamers. Such initial perturbations would be able to quickly develop into streamers and control the macroscopic electric field distribution even when a significant ambient electron density is present, and it is obvious that the significantly lower densities formed below sprite halo in the +CG case mentioned above would be highly favorable for development of nonoverlapping avalanches into streamers.

[21] The final factor, that is especially important for long-delayed sprites and sprites initiated by a continuing current, is that sprite halo produced by a +CG dynamically creates a region with $E > E_k$ that has very low electron density and can persist for tens of milliseconds creating highly favorable conditions for initiation of sprite streamers. This region appears to be a unique property of +CG produced halos and does not exist for -CG produced halos. In the +CG case the electrons move upward and against the downward descent of the halo. Due to the attachment processes just below the halo in the $E < E_k$ region and upward electron flux, the density of electrons becomes too low to support further halo advancements, and halo stops, even though the field remains above the breakdown field. The subsequent sections of the paper will provide quantitative illustration of this effect, that is especially important for initiation of long-delayed sprites.

3. Model Formulation

3.1. Improved Avalanche-to-Streamer Transition Criterion

[22] Numerical simulations of sprite-halo events using two-dimensional fluid model encounter difficulty if the plasma density is too low to be considered as a fluid. This problem appears, for example, in the low ambient electron density region when the halo development forms an electron attachment dominated region of low conductivity at low altitudes where the dynamics is on the particle level (i.e., distance between electrons becomes comparable to the grid resolution). In fact, regardless of the polarity of the lightning, low resolution can introduce a numerical instability as soon as the fluid model fails to simulate the dynamics of these sparse particles correctly. This instability can be somewhat postponed but not eliminated by increasing resolution of numerical grid. Given the broad range of length scales involved in the problem, and the related numerical requirements, an alternative way is to use a one-dimensional fluid model and then to employ a criterion on the particle level to check possible initiation of sprite streamers in the low-conductivity region. The one-dimensional model naturally avoids the instability and has a high enough resolu-

tion to guarantee the accuracy of the solution. Hence, based on the Meek's condition [e.g., Meek, 1940; Montijn and Ebert, 2006] we introduce an improved avalanche-to-streamer transition criterion, which allows arbitrary either time or spatial variation of the applied electric field. To gain additional physical insight, this criterion has also been used to monitor the development of electron avalanches in the high-conductivity region.

[23] An avalanche of electrons is approximated by a sphere with time-dependent radius R_a that is described by the ordinary differential equation:

$$\frac{dR_a}{dt} = \mu_e E' + \frac{2D_e}{R_a} \quad (1)$$

where μ_e and D_e are the mobility and the diffusion coefficient of electrons, respectively, and $E' = \frac{q_e N_e}{4\pi\epsilon_0 R_a^2}$ is the space-charge field of the avalanche, where N_e and q_e represent the total number of electrons inside the avalanche and the absolute value of the charge of the electron, respectively. The first term on the right-hand side of equation (1) describes expansion of the electron avalanche due to electrostatic repulsion. The second term accounts for effects of diffusive spreading of the avalanche. We note that in the absence of repulsion force the solution of equation (1) correctly captures classic diffusive expansion of the radius $R_a^2 = R_{a0}^2 + 4D_e t$, where R_{a0} is effective initial radius of electron cloud. The initial avalanche size R_{a0} do not affect the results as long as it is chosen so that the initial space-charge field of the avalanche is much smaller than the breakdown field. The time dynamics of N_e is described by the following equation:

$$\frac{dN_e}{dt} = (\nu_i - \nu_a) N_e \quad (2)$$

where ν_i and ν_a are ionization and two-body dissociative attachment frequencies, respectively. Three-body attachment processes are negligible at air pressure corresponding to mesospheric/lower-ionospheric altitudes studied in this paper. In our simulations, we assume that $E' \geq E_k/3$ corresponds to the avalanche-to-streamer transition [Raizer, 1991, section 12.2.6]. This is a simple criterion that indicates that electric field created by space-charge effects becomes comparable to the conventional breakdown field E_k . The specific choice of the $E_k/3$ reference is supported by high-resolution fluid simulations of avalanche-to-streamer transition indicating that once the space-charge field reaches $E_k/3$ it increases up to $5E_k$ very quickly. Equations (1) and (2) are solved numerically. We note that results of the present work are not sensitive to the specific values of initial avalanche radius as soon as these values are chosen to be much smaller than the final radius corresponding to avalanche-to-streamer transition.

[24] In practical calculations, it is convenient to apply equations (1) and (2) in two limited cases. When the propagation length of avalanches can be considered small in comparison with the characteristic spatial scale of the driving electric field, the avalanche development can be studied locally assuming homogeneous, but time-dependent, applied electric field $E(t)$. The time-dependent model quantities $\mu_e(t)$, $D_e(t)$, $\nu_i(t)$ and $\nu_a(t)$ at each location are calculated as functions of reduced electric field $E(t)/N$, where N is local air

density, using formulations of *Morrow and Lowke* [1997]. This local time-dependent regime applies to the early stage of sprite halos, which are developing at high altitudes where ambient electron density is high and dielectric relaxation time is short. For a time-independent electric field with spatial scale comparable to the propagation length of avalanches, the avalanches can be monitored starting from initial seeds and developing through the spatially dependent high-field region. The spatially dependent (usually only vertical coordinate/altitude-dependent) model quantities $\mu_e(\vec{r})$, $D_e(\vec{r})$, $\nu_i(\vec{r})$ and $\nu_a(\vec{r})$ are calculated by using reduced electric field $E(\vec{r})/N(\vec{r})$ at each location along the avalanche trajectory and for this purpose we assume in equations (1) and (2) that $dt = \frac{dr}{\mu_e E(\vec{r})}$, where \vec{r} is the spatial coordinate of the avalanche. This time-independent but spatially dependent regime applies to later stage of sprite halo, which evolves much slower due to low electron density. The above two cases are referred to as local criterion and spatial criterion, respectively.

3.2. Fluid Model

[25] In the present work, halos are simulated using a quasi-static electric model [e.g., *Pasko et al.*, 1995, 1997]. In order to simulate the motion of charged species, we solve drift-diffusion equations coupled with Poisson's equation, similarly to the approach described by *Luque and Ebert* [2009]:

$$\frac{\partial n_e}{\partial t} + \nabla \cdot (n_e \vec{v}_e - D_e \nabla n_e) = (\nu_i - \nu_a) n_e + S_{ph} \quad (3)$$

$$\frac{\partial n_p}{\partial t} = \nu_i n_e + S_{ph} \quad (4)$$

$$\frac{\partial n_n}{\partial t} = \nu_a n_e \quad (5)$$

$$\nabla^2 \phi = -\frac{q_e}{\epsilon_0} (n_p - n_e - n_n) \quad (6)$$

where n_e , n_p , and n_n are the electron, positive ion, and negative ion number densities, respectively, \vec{v}_e is the drift velocity of electrons, S_{ph} is the rate of electron-ion pair production due to photoionization, ϕ is the electric potential, and ϵ_0 is the permittivity of free space. The electron drift velocity is defined as $\vec{v}_e = -\mu_e \vec{E}$, where $\vec{E} = -\nabla \phi$ is the electric field. Ions are assumed to be motionless on the time scales considered in the present paper. Similarly to the avalanche-to-streamer transition model of section 3.1, the electron mobility μ_e , diffusion coefficient D_e , and the ionization ν_i and two-body attachment ν_a frequencies are defined as functions of the reduced electric field E/N using formulations of *Morrow and Lowke* [1997]. For computational efficiency a first-order donor cell scheme is used [*Dhali and Williams*, 1987]. An important feature of the present work is that it includes in halo modeling the fully self-consistent computation of the photoionization processes using the three-group SP₃ model developed by *Bourdon et al.* [2007] and *Liu et al.* [2007].

[26] In this work, in order to understand both spatial features and evolution of sprite halo during long time period, we have developed two codes: a two-dimensional (2-D) axisymmetric code in which we can analyze the radial features of the halos, and a one-dimensional (1-D) code that allows for obtaining an unprecedented spatial resolution avoiding unphysical small-scale instabilities and allowing to simulate the halo features during long temporal development. The simulation domain of the 2-D model extends from the ground and up to 95 km, and has a radius of 95 km. It is discretized using a numerical cylindrical (r, z) grid with 400×400 points corresponding to a resolution of $\Delta z = \Delta r = 237.5$ m. We use the same altitude range in the 1-D model, with a uniform one-dimensional grid in z direction with a spatial resolution of $\Delta z = 0.95$ m. Concerning the boundary conditions, we use the perfectly conducting boundary condition for all the boundaries in both 1-D and 2-D models. We verified the convergence of the results obtained with the 1-D model by increasing the spatial resolution of the numerical grid.

[27] In the 2-D model, the source charge Q in the thunderstorm is assumed to have a Gaussian distribution with a radius of 3 km and position at altitude $h_Q = 10$ km. For each Qh_Q change, we calculate the electric field by solving Poisson's equation in the simulation domain. In the 1-D model, for a given Qh_Q , the dynamic calculation of the electric field of source charge is taken from the 2-D model along the axis of symmetry. The space-charge field of the sprite halo is obtained by solving Poisson's equation, and the total field in the simulation domain is obtained by summing the space-charge field with the applied field for a given Qh_Q . We tested the consistency of 1-D and 2-D models by extending the horizontal distribution of the source charge in the 2-D model to a radius of 120 km (i.e., charge distribution was represented by a disc with radius 120 km) to simulate a quasi-1-D case. We verified that under these conditions the results of 2-D model coincide with those calculated by the 1-D model.

[28] We note that both 1-D and 2-D models cannot fully represent the dynamics of the sprite halo events. The results obtained by 2-D model suffer from convergence problems due to low resolution. Numerical instabilities appear when the sprite halo approaches low electron density but high electric field region. Simulations after this time are considered to be incorrect. The results obtained by 1-D model do not capture effects related to the radially distributed features of the sprite halo. Despite of these imperfections in the numerical models, analysis using coupling of avalanche-to-streamer transition criterion with large-scale electric fields obtained using the fluid model brings a new significant insight on the halo-sprite system.

3.3. Ambient Electron Density Profile

[29] The model ambient electron density n_e at altitude h is chosen to be in the standard form [*Wait and Spies*, 1964]:

$$n_e = n_{e0} e^{-0.15h'} e^{(\beta-0.15)(h-h')} \quad (7)$$

where $n_{e0} = 1.43 \times 10^{13} \text{ m}^{-3}$, and β [km^{-1}] and h' [km] are given parameters describing sharpness and reference altitude, respectively. We note that variation of parameter h'

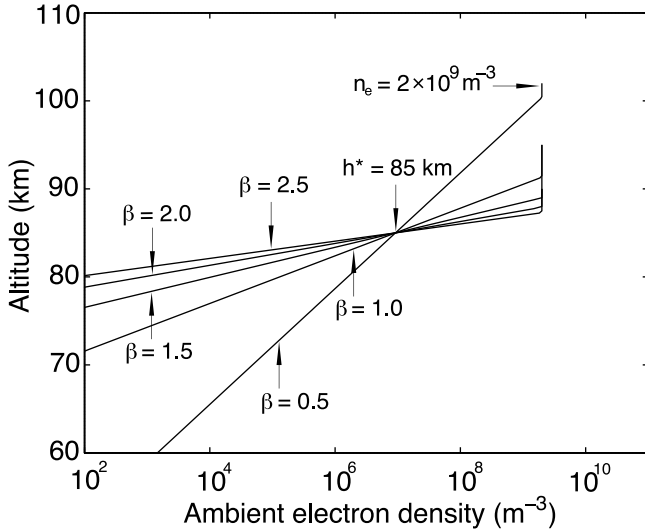


Figure 2. Ambient electron density profiles used in the present modeling. The quantity β is in km^{-1} .

allows vertical shifting of the electron density and conductivity profiles. The ambient electron density profiles used in this paper are represented in Figure 2. For a given lightning discharge duration τ_l the most significant electrodynamic response (i.e., related to development of space-charge effects) of the conducting atmosphere occurs just below an altitude h^* , where τ_l is equal to the dielectric relaxation time or Maxwell time ε_0/σ . Above this altitude, in the atmosphere with exponentially increasing conductivity as a function of altitude, the electric field will quickly relax. Below this altitude the electric field will persist and related effects will be observed as sprite halo. To avoid any additional complications related to changes in the altitude of this electrodynamic response (i.e., due to air density variations) and to focus on variability related to sharpness parameter β only, in our work we choose h^* to be constant and derive h' as a function of h^* and β . Therefore, as noted above, we define the parameter h^* by equating the duration of the return stroke τ_l and the dielectric relaxation time:

$$\tau_l = \frac{\varepsilon_0}{\sigma_e(h^*)} \quad (8)$$

where $\sigma_e(h) = \frac{q_e^2 n_e(h)}{m_e \nu_{em}(h)}$ is the ambient conductivity at altitude h , m_e is the mass of electron, and $\nu_{em} = \frac{q_e}{\mu_e m_e}$ is the effective collision frequency for momentum transfer. To obtain an analytical solution for h' as a function of h^* and β , we use a fit $\nu_{em} = \nu_0 e^{-0.15h}$, where $\nu_0 = 10^{13} \text{ s}^{-1}$, providing a good approximation of collision frequency of heated electrons in applied electric field on the order of E_k in the altitude range between 40 and 90 km. Then, we have $\sigma_e(h^*) = \sigma_0 e^{\beta(h^* - h')}$, where $\sigma_0 = \frac{q_e^2 n_{e0}}{m_e \nu_0} = 4 \times 10^{-8} \text{ S/m}$, and:

$$h' = h^* - \frac{1}{\beta} \ln \frac{\varepsilon_0}{\tau_l \sigma_0} \quad (9)$$

In our studies, h^* is chosen and β is the only independent parameter. The importance of the lightning duration τ_l has been demonstrated by Hiraki and Fukunishi [2006]. In the

present work, we assume that charge is removed linearly with time and fix $\tau_l = 1 \text{ ms}$ corresponding to a typical lightning duration [e.g., Pasko et al., 1997]. We also fix $h^* = 85 \text{ km}$ and choose $\beta = 0.5\text{--}2.4 \text{ km}^{-1}$. We note that the chosen range of variability of sharpness parameter β is consistent with variability of nighttime electron density profiles documented by Friedrich and Rapp [2009, Figure 11]. Generally, moving value of h^* to higher altitudes leads to reduction in Qh_Q values needed for electric field E to exceed the E_k threshold, while choosing h^* at lower altitudes leads to increase in Qh_Q values needed to achieve the $E > E_k$ condition at these lower altitudes with higher E_k values. The chosen value $h^* = 85 \text{ km}$ allows to illustrate and quantify all important effects intended in the present study, and similar analysis can be easily repeated for any other h^* value of interest.

4. Results

[30] Figure 3 shows the results calculated by the 2-D model for electron densities (Figures 3a–3b), the ratio E/E_k (Figures 3c–3d), and optical emissions from the first positive band system of N_2 ($B^3\Pi_g \rightarrow A^3\Sigma_u^+$) (Figures 3e–3f) at $t = 1 \text{ ms}$ in the sprite halos that are produced by the charge moment change $Qh_Q = 500 \text{ C km}$ for a +CG case, and the

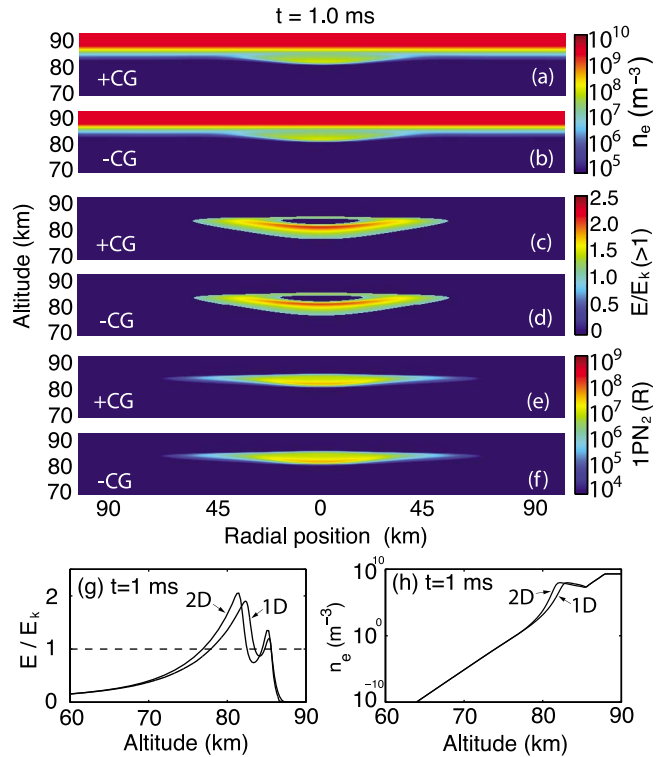


Figure 3. Cross-sectional views of (a–b) electron densities, (c–d) high-field regions of the reduced electric fields, and (e–f) optical emissions from 1PN_2 in positive and negative sprite halos given by the 2-D model for positive and negative CGs at $t = 1 \text{ ms}$ for a charge moment change $Qh_Q = 500 \text{ C km}$ and $\beta = 2.0 \text{ km}^{-1}$. The (g) ratios E/E_k and (h) electron densities at $t = 1 \text{ ms}$ calculated by the 1-D and 2-D models in the +CG case are also shown.

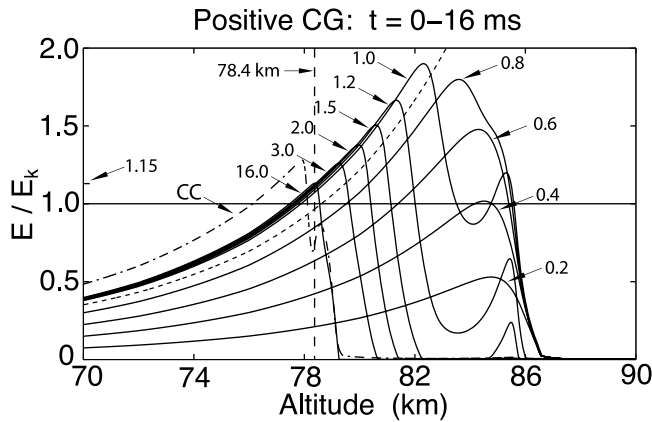


Figure 4. Evolution of the electric field in the mesosphere induced by a +CG from 0 to 16 ms simulated by the high-resolution 1-D model. In this case, $Qh_Q = 500 \text{ C km}$, and $\beta = 2.0 \text{ km}^{-1}$. The thick dashed line represents the ratio E_{amb}/E_k , where E_{amb} is the ambient electric field produced by the source charge in the underlying thunderstorm. The dot-dashed line labeled “CC” represents a model case with inclusion of the continuing current from 16 to 20 ms that contributes an extra 100 C km to the charge moment change produced by the +CG lightning. The thin vertical dashed line labeled “78.4 km” represents the approximate position of the space-charge distribution at the halo front at $t = 16 \text{ ms}$.

charge moment change $Qh_Q = -500 \text{ C km}$ for a -CG case, respectively. In both cases, the initial electron density profile is defined by the parameter $\beta = 2.0 \text{ km}^{-1}$. Figures 3a–3f show that the positive halo and negative halo at $t = 1 \text{ ms}$ appear to be identical, and both of them radially extend up to 70 km. Figures 3g–3h illustrate the difference between the 1-D and 2-D models in the +CG case. The sprite halo simulated by 2-D model develops slightly faster than the one in the 1-D model, and its electric field is slightly higher. These differences are related to focusing of electric field due to curvature of the halo in the 2-D case that is not captured by the 1-D model.

[31] Figures 4 and 5 show the evolution of E/E_k from the beginning of the return stroke and up to 16 ms calculated by high-resolution 1-D model for both polarities with identical physical parameters $|Qh_Q|$, h^* , and β . As can be clearly seen from Figures 4 and 5 before 2.0 ms, sprite halos produced by the +CG and the -CG are almost identical. Results of the simulation before $t = 2.0 \text{ ms}$ along with those presented in Figure 3 are similar to those reported by Pasko *et al.* [1997] and Asano *et al.* [2008, 2009], which stated a polarity independence of sprite initiation by lightning discharges. Further development between 2.0 and 3.0 ms shows that E/E_k in the sprite halos evolves much slower than for $t < 2.0 \text{ ms}$. After $t \approx 3 \text{ ms}$, the difference between two polarities becomes obvious. The change of E/E_k after 3 ms is so slow that the sprite halos seem to stop at these altitudes. It is interesting to note that E/E_k in the positive and negative case at 16 ms are significantly different from each other. In the sprite halo produced by +CG (positive halo), a region where the electric field is higher than E_k (high-field region) still exists, whereas in the negative case the electric field in the sprite

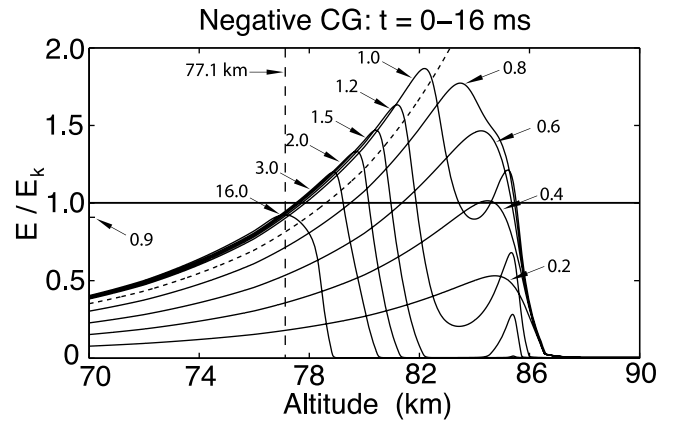


Figure 5. Evolution of the electric field in the mesosphere induced by a -CG from 0 to 16 ms simulated by the high-resolution 1-D model. In this case, $Qh_Q = 500 \text{ C km}$, and $\beta = 2.0 \text{ km}^{-1}$. The thick dashed line represents the ratio E_{amb}/E_k . The thin vertical dashed line labeled “77.1 km” represents the approximate position of the space-charge distribution at the halo front at $t = 16 \text{ ms}$.

halo produced by -CG (negative halo) is lower than E_k everywhere at this time. Note that the induced space charge is distributed around altitude approximately 77.1 km in the negative halo and around 78.4 km in the positive one at the same moment of time $t = 16 \text{ ms}$. The related altitudes are marked in Figures 4 and 5 by vertical dashed lines.

[32] In order to further investigate the asymmetry between positive and negative halo, Figure 6 presents a zoom-in view of the $E > E_k$ region of Figures 4 and 5 at $t = 1 \text{ ms}$ along with the charge densities. Figure 6 shows a downward shift of the space-charge distribution in the negative sprite halo compared to its positive counterpart, leading to slightly lower E/E_k in the negative halo. However, the differences between the positive and the negative halo at this moment of time are small, and they are not believed to be responsible for the polarity asymmetry of sprites at this stage of the halo development.

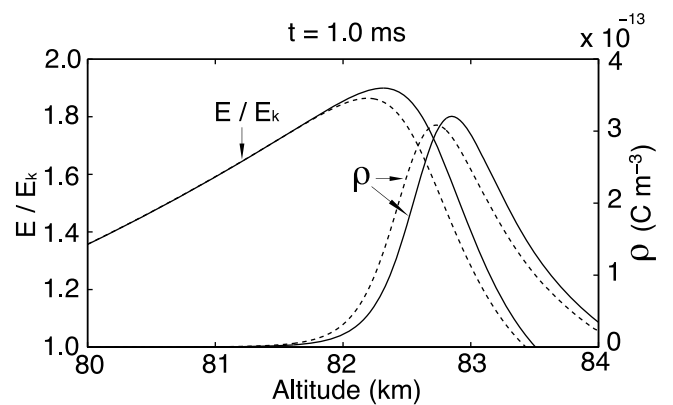


Figure 6. Charge density and reduced electric field distributions at $t = 1 \text{ ms}$ after the onset of the lightning stroke calculated by the high-resolution 1-D model. Solid lines represent the case of a +CG, and the dashed lines represent the case of a -CG.

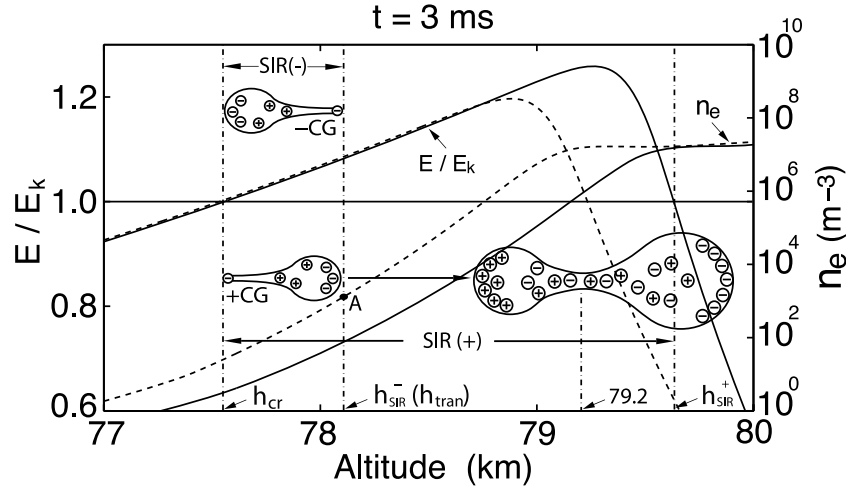


Figure 7. Electron density and reduced electric field distributions at $t = 3$ ms calculated by the high-resolution 1-D model using $Qh_Q = 500$ C km and $\beta = 2.0$ km $^{-1}$. Solid line represents halo induced by a +CG, and dashed line represents halo induced by a -CG. Dot “A” marks the altitude where the electron density is 10^3 m $^{-3}$ in the negative halo. The streamer initiation region (SIR) lies between the vertical dot-dashed lines at altitudes h_{cr} and h_{tran} (h_{SIR}^-) for the negative halo, and between altitudes h_{cr} and h_{SIR}^+ for the positive halo.

[33] Figure 7 presents the electric field and the electron density in the $E > E_k$ region of Figures 4 and 5 at $t = 3$ ms. The $E > E_k$ region of the negative halo between 77 and 80 km altitude is much smaller than that in the positive one. The lower parts of the $E > E_k$ regions of the positive and negative halos coincide with each other, whereas the upper boundary of the $E > E_k$ region of the negative halo appears at much lower altitude than that in the positive case. Meanwhile, the electron density in the $E > E_k$ region of the negative halo is approximately 2 orders of magnitude higher than that in the positive case.

[34] In Figure 8, we show the electron densities for both polarity cases at $t = 16$ ms to illustrate the effect of attachment processes. We also show the electron densities at $t = 16$ ms calculated by the model without photoionization under otherwise identical conditions. Figure 8 shows that attachment processes can greatly reduce the electron densities ahead of the sprite halo. Photoionization processes enhance the electron density by several orders of magnitude in a region just ahead of the sprite halo as emphasized in

Figure 8b. Note that electron attachment processes reduce the electron density smoothly ahead of the sprite halo, while the discrete nature of photoionization process in low-density regions may lead to formation of inhomogeneities ahead of the sprite halo. In this context it is useful to mention that the photoionization range of UV photons leading to photoionization of molecular oxygen molecules is $\simeq 55$ m and $\simeq 120$ m at altitudes 75 and 80 km, respectively [e.g., Liu and Pasko, 2004], and therefore the photoionization process is fully capable to create random seed electrons at distances of 100s of meters from high-field regions of sprite halo where related UV photons originate.

[35] For a given Qh_Q and β , 1-D model can provide E/E_k at every moment of time in the whole simulation domain as illustrated in Figures 4 and 5. Within the first several milliseconds from the onset of the return stroke, sprite halos propagate at high altitudes. At these altitudes (e.g., above 80 km in the cases studied in Figures 4 and 5) the ambient electron density is high and the dielectric relaxation time is very short. In such situation, we can combine the local

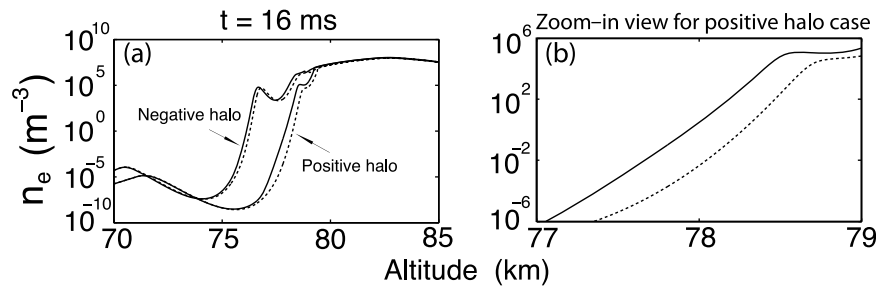


Figure 8. (a) Electron density at $t = 16$ ms calculated by the high-resolution 1-D model using $Qh_Q = 500$ C km and $\beta = 2.0$ km $^{-1}$. Solid line represents electron densities calculated by the model including photoionization, and dashed line represents electron densities calculated by model without photoionization. (b) Zoom-in view of the region between 77 to 79 km of the positive halo.

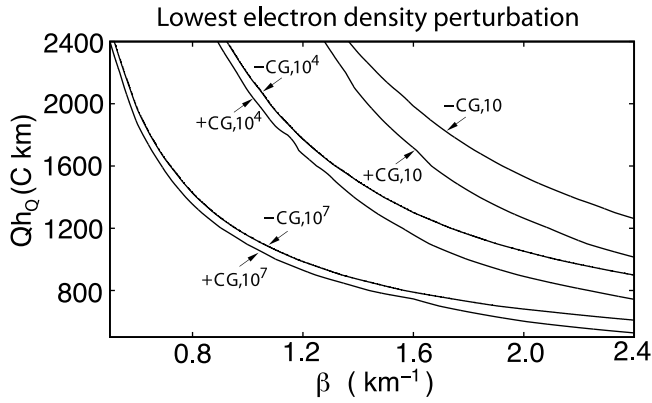


Figure 9. Lowest electron density perturbation N_{e0} required for triggering short-delayed sprites in the parametric space $Qh_0 - \beta$.

criterion (see section 3.1) and time-dependent electric field $E(t)$ to monitor the development of avalanches. At a given location, if $E(t) > E_k$, an electron avalanche is created, and the space-charge field E' produced by this avalanche is dynamically calculated using equations (1) and (2). If the local space-charge field E' of the avalanche can exceed $E_k/3$, we conclude that short-delayed (<3 ms) sprite streamers are triggered. Considering that electron density perturbations N_{e0} may exist in the ambient electron density, we also monitor the development of avalanches initiated from different representative numbers of seed electrons at each location. The quantity N_{e0} is interpreted as a relatively large number of electrons distributed in a compact region. For a selected set of $N_{e0} = 10, 10^4$ and 10^7 , we calculated

combinations of Qh_0 and β that are required for triggering of a short-delayed sprite streamer. The results are shown in Figure 9. All the simulations start from the onset of the lightning stroke and terminate at 3 ms to assure that the local criterion is valid. Figure 9 clearly shows that higher β requires lower Qh_0 to trigger sprite streamers, and high electron density perturbation can lower the requirements on both Qh_0 and β . The $-CG$ discharge generally has more stringent requirement for triggering short-delayed (<3 ms) sprites than the $+CG$ discharge, which is consistent with the results presented in Figures 4, 5 and 6 showing that E/E_k in the negative halo is lower than that in positive halo at a given time.

[36] It is important to note that the conditions depicted in Figure 9 are such that sprite streamers always occur at altitudes where distance between ambient electrons $L_e = n_e^{-1/3}$, where n_e is electron density, is longer than the avalanche radius R_a . Figure 10 illustrates this fact. In this case, we choose $\beta = 2.0 \text{ km}^{-1}$ and $Qh_0 = 1500 \text{ C km}$ with positive polarity in order to trigger a very short delayed sprite to assure that the local criterion is valid. Sprite streamers are triggered at $t = 1.1$ ms at 73.3 km where the space-charge field of an avalanche initiated from 10 seed electrons exceeds $E_k/3$. Note that at this altitude $L_e = 6.4$ m which is larger than the radius of avalanche $R_a = 3.4$ m when the avalanche-to-streamer transition occurs. At altitudes where $R_a > L_e$, avalanche-to-streamer transition cannot occur as illustrated at 77.5 km in Figure 10a by a vertical dashed line corresponding to $L_e = 2.3$ m and $R_a = 3.3$ m. The evolution of avalanche is illustrated in Figures 10b–10d at the altitude 73.3 km where streamer is triggered. The ambient electric field E exceeds E_k at about $t = 0.6$ ms. Although the radius of the avalanche keeps increasing during 0.6 to 1.0 ms,

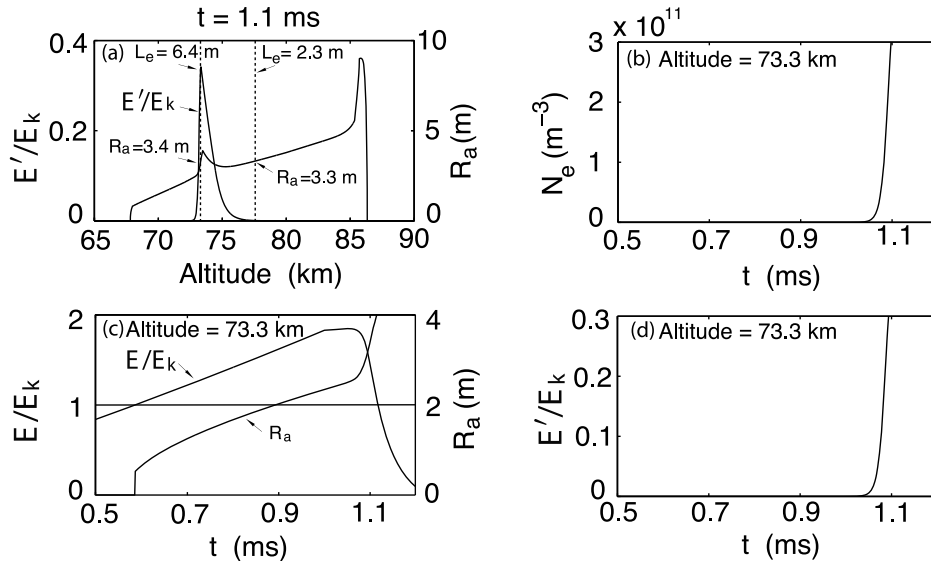


Figure 10. (a) The radius of avalanches R_a and the space-charge field of avalanches E' at different altitudes at $t = 1.1$ ms after the onset of return stroke calculated using the local avalanche approximation. The distance L_e represents the initial distance between ambient electrons at specific altitudes. In this simulation, $Qh_0 = +1500 \text{ C km}$, and $\beta = 2.0 \text{ km}^{-1}$. (b–d) Temporal evolution of an avalanche initiated from 10 seed electrons at 73.3 km, where Figure 10b shows the total number of electrons inside the avalanche, Figure 10c shows the applied electric field E/E_k at 73.3 km and the radius of the avalanche, and Figure 10d shows the space-charge field E'/E_k of the avalanche.

the fast multiplication of the electrons inside the avalanche occurs during 1.0 to 1.1 ms when the applied electric field is relatively high.

5. Discussion

5.1. Polarity Symmetry of +CGs and –CGs in Producing Sprite Halos

[37] Based on the results shown in Figures 4 and 5, we emphasize that above 80 km where positive halo and negative halo are almost identical, the ionization process proceeds in a diffuse/halo form, when high preionization leads to effective overlap among avalanches preventing streamer formation. In the results corresponding to Figure 4, examining the electron density at 80 km at the moment of time just before the $E > E_k$ region reaches this altitude, that is at $t \simeq 0.8$ ms, shows that the average distance between the seed electrons $L_e = 0.11$ m. This distance is slightly increased due to the attachment process compared to the initial distance, which is 0.10 m before the return stroke occurs. Calculation based on our local criterion (equations (1) and (2)) shows that the radius of the avalanche R_a initiated from a single seed electron at 80 km after the $E > E_k$ region (from $t = 0.8$ to $t = 2.5$ ms) passed through is 7.9 m. During this 1.7 ms duration, the electrons propagate over about 240 m, which is much shorter than the size of the $E > E_k$ region that is several km as shown in Figure 4. This confirms that the local criterion is a good approximation. The above analysis indicates that since $R_a \gg L_e$ the avalanches developing above 80 km can effectively overlap with each other and keep a smooth front ahead of the halo. However, local criterion fails below 80 km because low electron density leads to long persistent $E > E_k$ region and avalanches can propagate over a long distance. We find that $L_e = 0.21$ m at 79 km, $L_e = 0.39$ m at 78 km, and $L_e = 0.71$ m at 77 km measured at 0.8 ms are close to the order of magnitude of the characteristic streamer radius (several meters) at 75 km [Pasko *et al.*, 1998]. This implies that at these altitudes, the mechanism of overlapping of avalanches responsible for the disabling of streamer formation does not operate and sprite streamers can be triggered. Conclusions of the above analysis are also applicable to the negative case. Based on similar simulations, we find that in the diffuse halo regions where the avalanches effectively overlap with each other, there is only a slight polarity asymmetry between positive and negative halos corresponding to the same Qh_O due to the different charge distributions in negative and positive halos as shown on Figure 6. This asymmetry is related to the opposite direction of motion of electron, in positive and negative halos, and is weak precisely because the system is almost purely local at high electron density region. This is consistent with the observations of Miyasato *et al.* [2002] which show that spatiotemporal structure of halo events is very similar for both polarities.

5.2. Polarity Asymmetry of +CGs and –CGs in Triggering Sprite Streamers

[38] The ratio E_{amb}/E_k produced by the source charge in the underlying thunderstorm increases exponentially with altitude due to the neutral density variation, as shown in Figures 4 and 5. For a given Qh_O , if the ambient electron density is still too high around the altitude h_{cr} where $E_{amb} =$

E_k the avalanches will overlap and only diffuse sprite halo will be produced. For example, the conditions $Qh_O = 1000$ C km and $\beta = 0.5$ km⁻¹ with no continuing current are not able to initiate sprite streamers. The streamer formation ahead of the sprite halo front is possible only if the electron density is sufficiently low so that $L_e \gtrsim R_a$, where R_a is the radius of the avalanche at the avalanche-to-streamer transition, and h_{cr} is low enough to ensure that high electric field and growth of electron avalanches can occur in this region. Thus, for short-delayed sprites, it is insightful to consider that a sprite streamer could occur if condition $h_{tran} \gtrsim h_{cr}$ is fulfilled, which makes a link between the charge moment change Qh_O (defining h_{cr}) and the electron density profile (defining h_{tran}) in the lower ionosphere. Our calculations based on equations (1) and (2) show that the typical radius of avalanche just before the avalanche-to-streamer transition at 70–80 km is several meters (see, for example, Figure 10a). An estimate of h_{tran} can be made considering two effects. Firstly, if L_e is just slightly below 1 m, sprite streamers may still be triggered from inhomogeneities (i.e., electron density perturbations). Secondly, the altitude where the electric field equals to breakdown field is slightly lowered by space-charge effects compared to the original h_{cr} that is calculated by the source charge removed from the thundercloud. Therefore, in order to establish a practical numerical reference for L_e we assume that h_{tran} is the altitude where the distance between ambient electrons $L_e \simeq 0.1$ m corresponding to an electron density 10^3 m⁻³ = 10^{-3} cm⁻³. Figures 4 and 5 show that below 80 km, where ambient electron density is lower than 10^3 m⁻³, the electric field persists for a long time and thus provides a region for streamers to be triggered. This confirms that the altitude where $L_e = 0.1$ m is a good approximation for h_{tran} . The relations between SIR that we discussed in section 2 and the h_{cr} to h_{tran} region are different for positive and negative polarity. In Figure 1, for negative polarity, SIR and the h_{cr} to h_{tran} region are identical, whereas for positive polarity, SIR is larger than the h_{cr} to h_{tran} region. These different relations account for the polarity asymmetry of +CGs and –CGs in triggering sprite streamers as discussed in section 2.

[39] In order to illustrate an application of the above described conditions, we mention here the case documented by Hu *et al.* [2002] for which a +CG with $Qh_O = 120$ C km triggers a sprite within 6 ms time delay. Calculation of E_{amb} shows that in this event $h_{cr} = 87.5$ km. This result indicates that triggering of this short-delayed sprite requires the electron density to be lower than 10^3 m⁻³ around 87.5 km. This requirement is extremely stringent, and therefore this kind of short-delayed sprites, that is triggered by extremely low charge moment changes, rarely occurs. In the case studied in Figures 4 and 5, $h_{cr} = 78.6$ km defined by E_{amb} and $h_{tran} \simeq 80$ km defined by ambient electron density, which satisfies the approximate criterion to trigger short-delayed sprite. When the halo gets lower than 80 km, the large-scale ionization wave becomes unstable. Since the altitude h_{tran} is just slightly higher than h_{cr} , inhomogeneity in the electron density is critical in triggering of streamers. Streamer is triggered if an avalanche initiated from a perturbation succeeds to develop in the $E > E_k$ region fast enough for its space-charge field to exceed $E_k/3$.

[40] In order to examine possible sprite initiation in realistic cases, based on the analysis presented in section 2, we implement our spatial Meek's criterion using the results of

simulation corresponding to Figure 7 (or Figures 4 and 5 at $t \geq 3$ ms) in order to monitor the development of avalanches in low electron density region for both halo polarities. In this case, only the spatial criterion can describe the avalanche process because the propagation length of the avalanche is on the order of the spatial scale of the high-field region. Dielectric relaxation time at these low electron density altitudes is longer than the time required for the streamer formation. Note that once the ionization wave has reached altitudes below 80 km, the dynamics of the electric field evolves much slower due to low ambient electron density (see Figure 2) and low E/E_k (see Figures 4 and 5). This slow movement agrees with the high time-resolution observations [e.g., Moudry et al., 2003; Stenbaek-Nielsen and McHarg, 2008; Stenbaek-Nielsen et al., 2010a] showing that the downward movement of halo slows down and stops near the time of streamer formation. In Figure 7, we define the altitude h_{cr} as the lowest limit of the streamer initiation region (SIR) for both halo polarities, altitude h_{tran} (h_{SIR}^-) as the highest limit of the SIR for negative halo due to electron density being higher than 10^3 m^{-3} above this altitude, and altitude h_{SIR}^+ as the highest possible limit of the SIR for positive halo. Note that if an avalanche is initiated from a dense inhomogeneity, then when it reaches high altitude, its electron density is higher. In such a case, compared to an avalanche initiated from a lower-density inhomogeneity, this avalanche can penetrate into higher altitude, which means h_{SIR}^+ is higher. Therefore, the altitude h_{SIR}^+ is not only defined by E/E_k but also by the initial inhomogeneity as well as the growing ambient electron density. The SIR of the positive halo is between h_{cr} and h_{SIR}^+ , whereas the SIR of the negative halo is between h_{cr} and h_{SIR}^- . Calculations based on the spatial criterion confirm that in the positive halo case when an avalanche initiated from 10^2 seed electrons at altitude h_{cr} reaches altitude 79.2 km ($< h_{SIR}^+$), which is slightly lower than the peak of E/E_k , the space-charge field of the avalanche is $E' = 0.4E_k > E_k/3$ (Meek's criterion is fulfilled), and the electron density inside the avalanche is $8.0 \times 10^7 \text{ m}^{-3}$, which is 2 orders of magnitude higher than the electron density $n_e = 7.6 \times 10^5 \text{ m}^{-3}$ in the positive halo at 79.2 km. We note that 10^2 electrons is the minimum number of seed electrons that is needed for initiation of the streamers in the specific case considered. Avalanches initiated from inhomogeneities that are lower than 10^2 seed electrons would encounter a region with higher ambient electron density than that present in the avalanche before their space-charge field exceeds $E_k/3$. Once initiated, positive head of the streamer goes downward and grows up in the SIR very quickly. Generally, since the maximum luminosity of the halo is expected to appear at altitude slightly above the altitude of the peak electric field in the halo [e.g., Celestin and Pasko, 2010], while the streamer may be triggered at any locations of the $E > E_k$ region, a gap can exist between the sprite halo and the sprite streamer luminosity. The luminosity of the streamer head becomes detectable after sufficient propagation in the $E > E_k$ region [Stenbaek-Nielsen et al., 2007; Liu et al., 2009], which can increase this visible gap. This phenomenon is consistent with the observations of the vertical offset of sprite streamers with respect to sprite halo [McHarg et al., 2002; Moudry et al., 2003]. The negative head moves up and finally encounters the low-field and high-conductivity region, forming the diffuse part of sprites. We

consider that the random time and location of the appearance of compact seed distributions accounts for the time delay between halo event and sprite streamers as well as the lateral offset of streamers with respect to the underlying lightning [Wescott et al., 2001].

[41] In the negative halo, the SIR is shown in Figure 7 as appearing between the altitudes h_{SIR}^- and h_{cr} . Note that h_{SIR}^- is the altitude where average distance between the ambient electrons is 0.1 meter. Therefore, in the negative halo $h_{SIR}^- \equiv h_{tran}$. Overlapping among avalanches prevents the inception of streamers initiating at altitudes higher than h_{SIR}^- . In fact, the abundance of the seed electrons above altitude h_{SIR}^- produced by the halo tends to make a smooth front rather than filamentary streamers. Only the avalanches between altitude h_{SIR}^- and h_{cr} may succeed to develop without significant overlapping and can lead to the formation of space-charge fields E' to exceed $E_k/3$. We emphasize that in the case depicted in Figure 7 this condition is not satisfied even for avalanches initiated from perturbation as high as 10^{10} seeds.

5.3. Long-Delayed Sprite as Unique Property of +CGs

[42] For a given ambient electron density profile, if the charge moment change is high enough so that $h_{tran} \geq h_{cr}$, short-delayed sprites are triggered as soon as the development of sprite halo forms a low electron density region above h_{cr} . In contrast with this situation, if $h_{tran} < h_{cr}$ after the initial lightning discharge with a short duration, a continuing current is required to lower h_{cr} . Sprite initiation in this case is usually associated with longer time delays from the return stroke. Although it is obvious that continuing current can lower h_{cr} , the problem of sustaining a high-field ($E > E_k$) region during long time delay has not yet been addressed. In the case depicted in Figures 4 and 5, after $t = 3$ ms, both the positive and negative halo propagate much slower, and gradually stop as a quasi-steady state develops at altitudes corresponding to $E_{amb} \simeq 0.9E_k$. Figures 4 and 5 clearly demonstrate that after 16 ms, the positive halo still has a high-field region, whereas the negative halo does not. In fact, the high-field region disappeared before 10 ms in the -CG case. Note that the space-charge distribution appears at lower altitudes in the negative case (77.1 km) than that in the positive case (78.4 km). This downward shift results in lower ratio E/E_k in the negative case that is mostly defined by strong altitude variation of E_k proportionally to ambient air density. Indeed, we note that $E/E_k \simeq 1.15$ at 78.4 km altitude for the positive case (Figure 4) and $E/E_k \simeq 0.9$ at 77.1 km altitude for the negative case (Figure 5). Although for the same Qh_0 magnitudes in positive and negative cases the applied field E is nearly identical, the value of E_k is a factor of 1.24 higher at altitude 77.1 km in comparison with 78.4 km (this difference is defined by changes in ambient air density), directly accounting for 1.15/0.90 $\simeq 1.28$ difference in E/E_k values observed in Figures 4 and 5. The difference between dynamics of the two halos in the case of long-delayed sprites comes from the fact that at these low altitudes the electron flux and attachment play essential roles in the dynamics of the halo compared to the ionization processes. In the case of positive halos, electrons move from the already low electron density region at lower altitudes to high electron density region at higher altitudes. Once the electron density is too low to support further halo propagation due to the decreasing electron density and

attachment processes ahead of the halo, the halo stops even though the field is still higher than the breakdown field. In this quasi-stationary low electron density but high-field region, a perturbation can form sprite streamers and break the balance. This quasi-steady high-field region can last tens of milliseconds in our simulations and only weakens a little. The size of this region depends on the ambient electron density around the critical altitude h_{cr} above which $E > E_k$. Higher electron density around this altitude leads to a smaller altitude extent of the high-field region. No matter how small, this high-field region can exist for very long periods as long as $h_{cr} \ll h^*$, and can be noticeably enlarged by continuing current as shown by the dot-dashed line in Figure 4. In contrast, in the negative halo the electron flux comes from the high electron density region to the low electron density region. Even if the ionization is negligible, and the electric field is only slightly higher than the breakdown field, the electrons at high altitude would keep moving down. The negative sprite halo finally stops when electric field becomes lower than the breakdown field and electrons are quickly attached to ambient neutral gas.

[43] The altitude of the quasi-steady high-field region in positive halo depends on the total charge moment change Qh_Q . Our simulations demonstrate that continuing current increases the total Qh_Q and pulls the $E > E_k$ region down to lower altitude where electron density is lower, thus greatly enhances the possibility of triggering streamers by providing the opportunity for electron avalanche to occur in low electron density region.

[44] The dot-dashed line in Figure 4 is a representative result of these simulations involving continuing current. The $E > E_k$ region around 77 km at $t = 20$ ms is greatly enlarged by the continuing current from 16 to 20 ms that contributes to an additional 100 C km charge moment change. Considering the size of the high-field region and the lower electron density at these altitudes compared to the situation at $t = 3$ ms, sprite streamers can be readily triggered from an inhomogeneity by this continuing current. The lower onset altitude of sprite streamers in this case agrees with the observations documented by *Li et al.* [2008], which show that long-delayed sprites are generally initiated around 5 km lower than short-delayed sprites. In particular, with no continuing current, the electron density just below the stopped halo, where $E_{amb} \approx 0.9E_k$, can be greatly reduced by attachment processes. Once continuing current appears and pulls the $E > E_k$ region down to this area, sprite streamers can be easily initiated. Namely, compared to short-delayed sprites, for which initiation requires that $h_{tran} \gtrsim h_{cr}$, long-delayed sprites can be triggered in two ways. One way is that continuing current keeps flowing after the return stroke and pulls the $E > E_k$ region down to the altitudes where electron density is low enough; or attachment processes create a low electron density region just below the stopped sprite halo during long time delay, and then the appearance of relatively strong continuing current pulse enhances the electric field in this region and sprite streamers then can be initiated.

[45] We have also verified in our simulations that the long-duration lightning discharges ($\tau_l \gg 1$ ms, e.g., 5 ms) involving the same total charge moment change Qh_Q produce comparable size of quasi-steady high-field region at lower altitudes where streamers formation is allowed. This

is due to the fact that dielectric relaxation time in the low electron density region is much longer than τ_b , and therefore the change of τ_l does not affect the relaxation process at low altitudes much (i.e., the quasi-steady high-field region at low altitudes persists much longer than the lightning duration). However, long lightning duration results in low electric field at high altitudes, leading to dimmer halos that might not be detected. In this case, only sprite streamers could be observed. This result is consistent with the observation reported by *Adachi et al.* [2008], which shows that a 10 ms duration +CG corresponding to a charge moment change of ~ 1300 C km produced sprite streamers without a discernible halo. To summarize, for a given ambient electron density profile, the possibility of producing detectable sprite halo depends on the impulsive characteristics of the +CG lightning return stroke. The possibility of triggering sprite streamers mostly depends on the total charge moment change Qh_Q and the perturbations in the electron density (N_{e0}).

5.4. Origin of the Different Sprite Morphologies

[46] Based on the above analysis, we propose that the morphology of sprites mostly depends on the size of the SIR. The size of the SIR depends on h_{cr} and h_{tran} , that is, the charge moment change Qh_Q and, mainly, the electron density profile. If the size of the SIR is so small that avalanche-to-streamer transition occurs very close to upper boundary of the SIR, the luminosity of the upward negative streamer head could not be high enough to be observed. Only the downward part would be visible. This case corresponds to the case of column sprite or ‘‘C-sprite’’ [e.g., *Stenbaek-Nielsen and McHarg*, 2008]. If the SIR is large enough for the transition to occur in the middle of this region, both upward and downward streamer heads can further develop and become detectable. This situation would correspond to the case of ‘‘carrot sprite’’ [e.g., *Stenbaek-Nielsen and McHarg*, 2008], or a ‘‘jellyfish’’ sprite when a large constellation of carrot sprites is formed [*Stenbaek-Nielsen et al.*, 2000].

5.5. Dependence of Sprite Initiation on Qh_Q , β and N_{e0}

[47] An electron density perturbation creates favorable conditions for the fulfillment of avalanche-to-streamer transition since the avalanches initiated from higher inhomogeneities can develop faster and their space-charge field can more readily exceed the $E_k/3$ value. In the work of *Wescott et al.* [2001], perturbations have been referred to as micrometeors which trigger random ionizing events and result in the lateral offset of the sprites from lightning discharges. The local criterion is adopted to derive results presented in Figure 9 to systematically check dependence of sprite initiation on Qh_Q , β and N_{e0} . Note that when the charge moment changes Qh_Q and β are high enough so that sprite streamers are triggered with very short time delays, local criterion is valid since sprite streamer is initiated before the avalanche propagates a relatively long distance. As illustrated in Figure 9, higher electron density perturbation N_{e0} requires lower Qh_Q and β to trigger short-delayed sprites. For a given N_{e0} , higher β require lower Qh_Q to trigger sprite streamers due to longer dielectric relaxation time (or higher h_{tran}). We have also verified in our simulations that the condition $h_{tran} \gg h_{cr}$ leads to delays of sprite

streamers with respect to the onset of lightning return stroke as short as 0.7 ms. With such short-delayed sprites, halos and sprites can appear almost simultaneously. We note that the enhancement of ionospheric conductivity during daytime would lower h_{tran} and result in higher electric field requirement, which is consistent with the observations reported by *Stanley et al.* [2000].

[48] Although Figure 9 provides an illustration of the dependence of sprite initiation on Qh_Q , β and N_{e0} , it is important to emphasize that this kind of extreme conditions (high charge moment changes within 1 ms, sharp gradient of ambient electron density, and strong inhomogeneities) do not usually occur. Once these extreme conditions are provided, polarity asymmetry between +CGs and -CGs corresponding to the same charge moment change in triggering sprite streamers should be much smaller than under typical conditions realized in reality, because the sprite streamer can be triggered locally, and the strong spatial asymmetries discussed in section 5.2 do not apply. In the case depicted in Figure 10, instead of a +CG, a -CG with $Qh_Q = -1500$ C km under condition of $\beta = 2.0$ km⁻¹ also can produce sprite streamers from slightly higher inhomogeneities (e.g., $N_{e0} = 10^2$). Nevertheless, we note that the charge distribution in halos leads to a slight asymmetry (see section 5.1) that is noticeable in Figure 9 and manifested in higher contour lines corresponding to -CG cases for a given electron density perturbation in comparison with +CG cases. We also emphasize that for these relatively large charge moment change values, asymmetry between occurrence probability of causative -CGs and +CGs can be significant.

6. Conclusions

[49] Principal contributions of this work can be summarized as follows:

[50] 1. We have developed a 2-D and a high-resolution 1-D plasma fluid model coupled with an improved Meek's criterion allowing quantitative investigation of possible initiation of sprite streamers in association with sprite halos that are produced by both +CGs and -CGs.

[51] 2. We have established a direct link between the charge moment change and the ambient electron density profile as required for triggering of sprite streamers. The related condition is defined as $h_{\text{tran}} \gtrsim h_{\text{cr}}$, where h_{tran} represents the altitude at which the electron density is low enough so that the distance between electrons is equal to the radius of the electron avalanche at the moment of avalanche-to-streamer transition, and h_{cr} represents the altitude at which the ambient electric field E_{amb} created by the charge moment change in the thunderstorm is equal to the breakdown field E_k . This points out that the requirement for triggering of sprite streamers is fulfilled if the ambient electron density along with the attachment processes form a low electron density region above the critical altitude h_{cr} , that allows the avalanches to develop without overlapping.

[52] 3. The polarity symmetry of +CGs and -CGs in producing sprite halos is demonstrated. During the sprite halo stage, the responses of the lower ionosphere to +CGs and -CGs are almost identical. As long as the electron avalanches effectively overlap with each other, no strong polarity asymmetry would appear in the positive and negative halo associated with otherwise identical external conditions.

[53] 4. Analysis of the origin of polarity asymmetry between +CGs and -CGs in triggering of sprite streamers has been carried out. The vertical extent of streamer initiation region (SIR) created by a -CG is smaller than the SIR created by the opposite +CG that corresponds to the same charge moment change. This is due to the fact that, the positive SIR is basically equivalent to the high-field $E > E_k$ region created by the halo because upward avalanches generated in a low electron density region can penetrate deep into the high electron density region of the halo. In contrast, the negative SIR is limited to the high-field region where the electron density is low enough for avalanches to develop without overlapping. The -CGs may produce short-delayed sprites in the unlikely event of extremely high charge moment change Qh_Q and ionospheric sharpness β parameter that fulfill the avalanche-to-streamer transition within a large enough SIR region.

[54] 5. Factors that determine the observational features of sprite streamers are also studied. For both lightning polarities, positive streamers have larger effective $E > E_k$ region to develop because they propagate in the opposite direction to the initial avalanches. Also, sprite streamers triggered by +CGs can propagate to significantly lower altitudes than those triggered by -CGs due to a factor of 3 lower minimum field required for propagation of positive streamers E_{cr}^+ in comparison with similar field E_{cr}^- for negative streamers.

[55] 6. We have investigated the evolution of high-field region in the halo produced by the lightning return stroke in the case of long delays, and the effect of the lightning continuing current on triggering long-delayed sprite streamers. A long-lasting quasi-steady high-field region has been discovered as a unique property of positive halos. The enlargement of this high-field region by continuing current is also demonstrated.

[56] 7. We also make suggestions on the conditions leading to the formation of sprites with different morphologies. We suggest that large streamer initiation regions in which both positive and negative streamers have room to grow produce "carrot sprites," whereas small ones only produce "C-sprites."

[57] 8. We have documented the dependence of initiation of sprite streamers on three parameters: charge moment change Qh_Q , electron density profile sharpness parameter β , and electron density perturbation N_{e0} . High values of Qh_Q , β and N_{e0} are favorable for sprite initiation. We also established that if charge moment change is extremely high (e.g., 2000 C km removed within 1 ms) and electron density is very low at lower altitudes (e.g., $\beta = 2.0$ km⁻¹), the sprite streamers can be triggered locally. In such cases, polarity asymmetry between +CGs and -CGs associated with the same charge moment change in triggering sprite streamers is much smaller than under realistic conditions typically expected during sprite observations.

Notation

Qh_Q Charge moment change defined as the amount of charge Q transferred to ground times the altitude h_Q from which the charge was removed.

τ_l Lightning discharge duration (in the present work assumed to be 1 ms).

- E_k Conventional breakdown field defined by the equality of the ionization and dissociative attachment frequencies.
- E_{cr}^{\pm} Applied electric field required for stable propagation of positive/negative streamer.
- E_{amb} Applied ambient electric field produced by a cloud-to-ground lightning discharge.
- Δh_{HALO} The altitude range where ambient electron density is high enough to sustain a discharge in a diffuse glow form (i.e., in a halo form).
- SIR Streamer initiation region: the region where electron avalanches may potentially transform into streamers.
- h_{cr} The altitude above which the applied ambient electric field E_{amb} is higher than the breakdown field E_k .
- h_{SIR}^{\pm} The highest-altitude limit of the streamer initiation region for positive/negative halo.
- h_{tran} The altitude above which the average distance between ambient electrons is shorter than the diameter of an avalanche at the moment of avalanche-to-streamer transition. In the case of negative cloud-to-ground lightning discharges, $h_{tran} \equiv h_{SIR}^-$.

[58] **Acknowledgments.** This research was supported by NSF grant AGS-0734083 and DARPA NIMBUS grant HR0011-101-0059/10-DARPA-1092 to Pennsylvania State University.

References

- Adachi, T., et al. (2008), Electric fields and electron energies in sprites and temporal evolutions of lightning charge moment measurements, *J. Phys. D Appl. Phys.*, *41*, 234010, doi:10.1088/0022-3727/41/23/234010.
- Asano, T., M. Hayakawa, M. G. Cho, and T. Suzuki (2008), Computer simulations on the initiation and morphological difference of Japan winter and summer sprites, *J. Geophys. Res.*, *113*, A02308, doi:10.1029/2007JA012528.
- Asano, T., T. Suzuki, Y. Hiraki, E. Mareev, M. G. Cho, and M. Hayakawa (2009), Computer simulations on sprite initiation for realistic lightning models with higher-frequency surges, *J. Geophys. Res.*, *114*, A02310, doi:10.1029/2008JA013651.
- Barrington-Leigh, C. P., U. S. Inan, M. Stanley, and S. A. Cummer (1999), Sprites triggered by negative lightning discharges, *Geophys. Res. Lett.*, *26*(24), 3605–3608, doi:10.1029/1999GL010692.
- Barrington-Leigh, C. P., U. S. Inan, and M. Stanley (2001), Identification of sprites and elves with intensified video and broadband array photometry, *J. Geophys. Res.*, *106*(A2), 1741–1750, doi:10.1029/2000JA000073.
- Bell, T. F., S. C. Reising, and U. S. Inan (1998), Intense continuing currents following positive cloud-to-ground lightning associated with red sprites, *Geophys. Res. Lett.*, *25*(8), 1285–1288, doi:10.1029/98GL00734.
- Bourdon, A., V. P. Pasko, N. Y. Liu, S. Celestin, P. Segur, and E. Marode (2007), Efficient models for photoionization produced by non-thermal gas discharges in air based on radiative transfer and the Helmholtz equations, *Plasma Sources Sci. Technol.*, *16*, 656–678.
- Celestin, S., and V. P. Pasko (2010), Effects of spatial non-uniformity of streamer discharges on spectroscopic diagnostics of peak electric fields in transient luminous events, *Geophys. Res. Lett.*, *37*, L07804, doi:10.1029/2010GL042675.
- Cummer, S. A., and M. Fullekrug (2001), Unusually intense continuing current in lightning produces delayed mesospheric breakdown, *Geophys. Res. Lett.*, *28*(3), 495–498, doi:10.1029/2000GL012214.
- Cummer, S. A., and W. A. Lyons (2005), Implication of lightning charge moment changes for sprite initiation, *J. Geophys. Res.*, *110*, A04304, doi:10.1029/2004JA010812.
- Cummer, S. A., N. C. Jaugey, J. B. Li, W. A. Lyons, T. E. Nelson, and E. A. Gerken (2006), Submillisecond imaging of sprite development and structure, *Geophys. Res. Lett.*, *33*, L04104, doi:10.1029/2005GL024969.
- Dhali, S. K., and P. F. Williams (1987), Two-dimensional studies of streamers in gases, *J. Appl. Phys.*, *62*, 4696–4707.
- Franz, R. C., R. J. Nenzek, and J. R. Winckler (1990), Television image of a large upward electric discharge above a thunderstorm system, *Science*, *249*, 48–51.
- Friedrich, M., and M. Rapp (2009), News from the lower ionosphere: A review of recent developments, *Surv. Geophys.*, *30*(6), 525–559, doi:10.1007/s10712-009-9074-2.
- Gerken, E. A., U. S. Inan, and C. P. Barrington-Leigh (2000), Telescopic imaging of sprites, *Geophys. Res. Lett.*, *27*(17), 2637–2640, doi:10.1029/2000GL000035.
- Gherardi, N., and F. Massines (2001), Mechanisms controlling the transition from glow silent discharge to streamer discharge in nitrogen, *IEEE Trans. Plasma Sci.*, *29*(3), 536–544.
- Hiraki, Y., and H. Fukunishi (2006), Theoretical criterion of charge moment change by lightning for initiation of sprites, *J. Geophys. Res.*, *111*, A11305, doi:10.1029/2006JA011729.
- Hu, W. Y., S. A. Cummer, and W. A. Lyons (2002), Lightning charge moment changes for the initiation of sprites, *Geophys. Res. Lett.*, *29*(8), 1279, doi:10.1029/2001GL014593.
- Hu, W. Y., S. A. Cummer, and W. A. Lyons (2007), Testing sprite initiation theory using lightning measurements and modeled electromagnetic fields, *J. Geophys. Res.*, *112*, D13115, doi:10.1029/2006JD007939.
- Li, J., and S. Cummer (2011), Estimation of electric charge in sprites from optical and radio observations, *J. Geophys. Res.*, *116*, A01301, doi:10.1029/2010JA015391.
- Li, J., S. A. Cummer, W. A. Lyons, and T. E. Nelson (2008), Coordinated analysis of delayed sprites with high-speed images and remote electromagnetic fields, *J. Geophys. Res.*, *113*, D20206, doi:10.1029/2008JD010008.
- Liu, N. Y., and V. P. Pasko (2004), Effects of photoionization on propagation and branching of positive and negative streamers in sprites, *J. Geophys. Res.*, *109*, A04301, doi:10.1029/2003JA010064.
- Liu, N. Y., S. Celestin, A. Bourdon, V. P. Pasko, P. Segur, and E. Marode (2007), Application of photoionization models based on radiative transfer and the Helmholtz equations to studies of streamers in weak electric fields, *Appl. Phys. Lett.*, *91*, 211501, doi:10.1063/1.2816906.
- Liu, N. Y., V. P. Pasko, K. Adams, H. C. Stenbaek-Nielsen, and M. G. McHarg (2009), Comparison of acceleration, expansion, and brightness of sprite streamers obtained from modeling and high-speed video observations, *J. Geophys. Res.*, *114*, A00E03, doi:10.1029/2008JA013720.
- Luque, A., and U. Ebert (2009), Emergence of sprite streamers from screening-ionization waves in the lower ionosphere, *Nat. Geosci.*, *2*(11), 757–760, doi:10.1038/NNGEO662.
- Luque, A., and U. Ebert (2010), Sprites in varying air density: Charge conservation, glowing negative trails and changing velocity, *Geophys. Res. Lett.*, *37*, L06806, doi:10.1029/2009GL041982.
- Marshall, R. A., and U. S. Inan (2006), High-speed measurements of small-scale features in sprites: Sizes and lifetimes, *Radio Sci.*, *41*, RS6S43, doi:10.1029/2005RS003353.
- Massines, F., A. Rabehi, P. Decomps, R. Gadri, P. Segur, and C. Mayoux (1998), Experimental and theoretical study of a glow discharge at atmospheric pressure controlled by dielectric barrier, *J. Appl. Phys.*, *83*, 2950–2957.
- McHarg, M. G., R. K. Haaland, D. R. Moudry, and H. C. Stenbaek-Nielsen (2002), Altitude-time development of sprites, *J. Geophys. Res.*, *107*(A11), 1364, doi:10.1029/2001JA000283.
- McHarg, M. G., H. C. Stenbaek-Nielsen, and T. Kanmae (2007), Streamer development in sprites, *Geophys. Res. Lett.*, *34*, L06804, doi:10.1029/2006GL027854.
- Meek, J. (1940), A theory of spark discharge, *Phys. Rev.*, *57*(8), 722–728.
- Miyasato, R., M. J. Taylor, H. Fukunishi, and H. C. Stenbaek-Nielsen (2002), Statistical characteristics of sprite halo events using coincident photometric and imaging data, *Geophys. Res. Lett.*, *29*(21), 2033, doi:10.1029/2001GL014480.
- Montijn, C., and U. Ebert (2006), Diffusion correction to the Raether-Meek criterion for the avalanche-to-streamer transition, *J. Phys. D Appl. Phys.*, *39*(14), 2979–2992, doi:10.1088/0022-3727/39/14/017.
- Morrow, R., and J. J. Lowke (1997), Streamer propagation in air, *J. Phys. D Appl. Phys.*, *30*, 614–627.
- Moudry, D. R., H. C. Stenbaek-Nielsen, D. D. Sentman, and E. M. Wescott (2003), Imaging of elves, halos and sprite initiation at 1 ms time resolution, *J. Atmos. Solar Terr. Phys.*, *65*, 509–518, doi:10.1016/S1364-6826(02)00323-1.
- Newsome, R. T., and U. S. Inan (2010), Free-running ground-based photometric array imaging of transient luminous events, *J. Geophys. Res.*, *115*, A00E41, doi:10.1029/2009JA014834.
- Palmer, A. J. (1974), Physical model on initiation of atmospheric-pressure glow discharges, *Appl. Phys. Lett.*, *25*(3), 138–140.
- Pasko, V. P., U. S. Inan, Y. N. Taranenko, and T. F. Bell (1995), Heating, ionization and thunder discharges in the mesosphere due to intense quasi-electrostatic thundercloud fields, *Geophys. Res. Lett.*, *22*(4), 365–368, doi:10.1029/95GL00008.

- Pasko, V. P. (2010), Recent advances in theory of transient luminous events, *J. Geophys. Res.*, *115*, A00E35, doi:10.1029/2009JA014860.
- Pasko, V. P., and H. C. Stenbaek-Nielsen (2002), Diffuse and streamer regions of sprites, *Geophys. Res. Lett.*, *29*(10), 1440, doi:10.1029/2001GL014241.
- Pasko, V. P., U. S. Inan, and T. F. Bell (1996), Blue jets produced by quasi-electrostatic pre-discharge thundercloud fields, *Geophys. Res. Lett.*, *23*(3), 301–304, doi:10.1029/96GL00149.
- Pasko, V. P., U. S. Inan, T. F. Bell, and Y. N. Taranenko (1997), Sprites produced by quasi-electrostatic heating and ionization in the lower ionosphere, *J. Geophys. Res.*, *102*(A3), 4529–4561, doi:10.1029/96JA03528.
- Pasko, V. P., U. S. Inan, and T. F. Bell (1998), Spatial structure of sprites, *Geophys. Res. Lett.*, *25*(12), 2123–2126, doi:10.1029/98GL01242.
- Pasko, V. P., U. S. Inan, and T. F. Bell (2000), Fractal structure of sprites, *Geophys. Res. Lett.*, *27*(4), 497–500, doi:10.1029/1999GL010749.
- Raizer, Y. P. (1991), *Gas Discharge Physics*, Springer, New York.
- Sentman, D. D., E. M. Wescott, D. L. Osborne, D. L. Hampton, and M. J. Heavner (1995), Preliminary results from the Sprites94 Aircraft Campaign: 1. Red sprites, *Geophys. Res. Lett.*, *22*(10), 1205–1208, doi:10.1029/95GL00583.
- Stanley, M., P. Krehbiel, M. Brook, C. Moore, W. Rison, and B. Abrahams (1999), High speed video of initial sprite development, *Geophys. Res. Lett.*, *26*(20), 3201–3204, doi:10.1029/1999GL010673.
- Stanley, M., M. Brook, P. Krehbiel, and S. A. Cummer (2000), Detection of daytime sprites via a unique sprite ELF signature, *Geophys. Res. Lett.*, *27*(6), 871–874, doi:10.1029/1999GL010769.
- Stenbaek-Nielsen, H. C., and M. G. McHarg (2008), High time-resolution sprite imaging: Observations and implications, *J. Phys. D Appl. Phys.*, *41*, 234009.
- Stenbaek-Nielsen, H. C., D. R. Moudry, E. M. Wescott, D. D. Sentman, and F. T. S. Sabbas (2000), Sprites and possible mesospheric effects, *Geophys. Res. Lett.*, *27*(23), 3829–3832, doi:10.1029/2000GL003827.
- Stenbaek-Nielsen, H. C., M. G. McHarg, T. Kanmae, and D. D. Sentman (2007), Observed emission rates in sprite streamer heads, *Geophys. Res. Lett.*, *34*, L11105, doi:10.1029/2007GL029881.
- Stenbaek-Nielsen, H. C., M. G. McHarg, and R. Haaland (2010a), High-speed observations of sprite halo and streamer onset, Abstract AE14A-03 presented at 2010 Fall Meeting, AGU, San Francisco, Calif., 13–17 Dec.
- Stenbaek-Nielsen, H. C., R. Haaland, M. G. McHarg, B. A. Hensley, and T. Kanmae (2010b), Sprite initiation altitude measured by triangulation, *J. Geophys. Res.*, *115*, A00E12, doi:10.1029/2009JA014543.
- Taylor, M. J., et al. (2008), Rare measurements of a sprite with halo event driven by a negative lightning discharge over Argentina, *Geophys. Res. Lett.*, *35*, L14812, doi:10.1029/2008GL033984.
- Vitello, P. A., B. M. Penetrante, and J. N. Bardsley (1994), Simulation of negative-streamer dynamics in nitrogen, *Phys. Rev. E*, *49*, 5574–5598.
- Wait, J. R., and K. P. Spies (1964), *Characteristics of the Earth-Ionosphere Waveguide for VLF Radio Waves*, Tech. Note 300, Natl. Bur. of Standards, Boulder, Colo.
- Wescott, E. M., H. C. Stenbaek-Nielsen, D. D. Sentman, M. J. Heavner, D. R. Moudry, and F. T. S. Sabbas (2001), Triangulation of sprites, associated halos and their possible relation to causative lightning and micrometeors, *J. Geophys. Res.*, *106*(A6), 10,467–10,478, doi:10.1029/2000JA000182.
- Williams, E., E. Downes, R. Boldi, W. Lyons, and S. Heckman (2007), Polarity asymmetry of sprite-producing lightning: A paradox?, *Radio Sci.*, *42*, RS2S17, doi:10.1029/2006RS003488.

S. Celestin, V. P. Pasko, and J. Qin, Communications and Space Sciences Laboratory, Department of Electrical Engineering, Penn State University, 227 EE East, University Park, PA 16802-2706, USA. (sebastien.celestin@psu.edu; vpasko@psu.edu; jianqin@psu.edu)